



Controls on the frequency content of near-source infrasound at open-vent volcanoes: a case study from Volcán Villarrica, Chile

Bryan B. Rosenblatt¹ · Jeffrey B. Johnson¹ · Jacob F. Anderson¹ · Keehoon Kim² · Scott J. Gauvain¹

Received: 24 May 2022 / Accepted: 14 October 2022
© International Association of Volcanology & Chemistry of the Earth's Interior 2022

Abstract

Infrasound signals from open-vent volcanoes can contain information related to that volcano's eruption dynamics and future activity. Studying a specific volcano's acoustic signature during periods of relative quiescence is thus important for understanding potential warning signs of impending eruptions. Volcán Villarrica, located in southern Chile, has a long-lived active lava lake that produces continuous infrasound with spectral peaks centered around 1 Hz that vary by $+/- \sim 0.2$ Hz over day-to-week-long time scales. The infrasound frequency content has been shown to illuminate key volcanic properties such as eruption style and crater shape. Leading up to Villarrica's most recent paroxysm in 2015, for instance, infrasound spectral changes coincided with a rise in Villarrica's lava lake level. Quantifying and understanding the regular fluctuation in recorded infrasonic frequencies from Villarrica and other open-vent volcanoes is thus imperative during periods of relative calm. Our experiment entailed a week-long period of crater rim infrasound observations associated with stable, open-vent activity and revealed two independent source processes: spatter bursting events (relatively broadband infrasound) and lava lake-induced tremor (sustained signals peaked at 1 Hz). A comparison of these acoustic signals with results from 3-D finite-difference time-domain wave propagation models shows that while sound speed variability can influence Villarrica's spectrum, it cannot explain the full extent of the observed frequency excursions. We conclude that source spectrum variability is primarily responsible for the frequency excursions. Our work highlights the utility of data collected from a dense distribution of twenty infrasound sensors operating at the summit coupled with numerical modeling of sound radiation.

Keywords Infrasound · Volcanoes · Open-vent · Lava lake · Villarrica · Crater acoustic resonance

Introduction

Editorial responsibility: S. Vergniolle

This paper constitutes part of a topical collection: Open-vent volcanoes

✉ Bryan B. Rosenblatt
Bryanrosenblatt@u.boisestate.edu

Jeffrey B. Johnson
JeffreyBJohnson@boisestate.edu

Jacob F. Anderson
Jacobanderson152@boisestate.edu

Keehoon Kim
kim84@llnl.gov

Scott J. Gauvain
scottgauvain@u.boisestate.edu

¹ Department of Sciences, Boise State University, Boise, ID, USA

² Lawrence Livermore National Lab, Livermore, CA, USA

Degassing and eruptive activity at most volcanoes produce infrasound (low-frequency acoustic waves below the 20 Hz threshold of human hearing), which can be used to characterize eruptive activity (e.g., Vergniolle and Caplan-Auerbach 2004; Dzierma and Wehrmann 2010; Ripepe et al. 2010; Goto and Johnson 2011; Allstadt et al. 2018; Vergniolle and Métrich 2022). Infrasound measurements, modeling, and wave inversions have been used to estimate the gas volume of Strombolian explosions at specific open-vent volcanoes such as Stromboli (Italy; Vergniolle and Brandeis 1994, 1996), Erebus (Antarctica; Johnson et al. 2008), Yasur (Vanuatu; Iezzi et al. 2019), and Santiaguito (Guatemala; Johnson et al. 2011), respectively. In addition, infrasonic power has been used to estimate the gas velocity and gas volume of eruptions at Shishaldin (Alaska; Vergniolle and Caplan-Auerbach 2006) and Augustine (Alaska; Caplan-Auerbach et al. 2010). Peaked infrasound spectra are

common for volcanoes, such as Cotopaxi (Ecuador), where infrasound was used to measure the dimension of the summit conduit during a period of activity in 2016 (Johnson et al. 2018a; Johnson & Watson 2019). Resonant infrasound from the craters of Mt. Etna (Italy; Spina et al. 2014), or the large, open-vent crater of Halema‘uma‘u (Kīlauea, Hawai‘i; Fee et al. 2010), have also been used to infer the lengths of their respective conduits.

One of the primary influences on a volcano’s infrasound radiation is the geometry of the vent region. This is especially the case for open-vent volcanoes, where the shape of volcanic craters has previously been described as that of a massive horn (Richardson et al. 2014; Johnson et al. 2018b; Watson et al. 2019) or a cavity that approximates a Helmholtz resonator (Fee et al. 2010; Goto and Johnson 2011; Spina et al. 2014) in which variations of a lava lake’s level can change the effective length of the volcanic conduit and influence the dominant peaks of radiated infrasound. As such, infrasonic pressure waves contain key information related to the dynamics of volcanic processes (e.g., Vergniolle and Brandeis 1994; Vergniolle and Caplan-Auerbach 2004; Marchetti et al. 2009; Spina et al. 2014). An approach to understanding the effects of a crater’s shape is to utilize numerical models to calculate Green’s functions, which may then be deconvolved from recorded signals (Johnson et al. 2018a; Watson et al. 2019, 2020). In addition to crater geometry, wave propagation models can also be used to implement and evaluate the effects of variable atmospheric temperature structures and a range of source-time functions (Kim and Lees 2011; Kim et al. 2012; Taddeucci et al. 2012; Lacanna and Ripepe 2013).

Variations of a lava lake’s level relate to changes in magma supply and are impacted by the depth-varying diameter of a volcanic conduit and crater. Geometries of craters and dynamics of active lava lakes vary broadly. The largest lava lakes, including Nyiragongo (Democratic Republic of Congo) and Halema‘uma‘u, are several hundred meters in diameter (Lev et al. 2019). Halema‘uma‘u’s lava lake has been observed directly through visual and thermal camera measurements, and its surface deformation is related to reservoir pressure occurring over time scales of weeks (Patrick et al. 2015). Nyiragongo’s lava lake has been a persistent source of degassing and infrasound radiation (Sawyer et al. 2008; Barrière et al. 2018), and large variations of its level have led to rapid drainage events along rifts occurring with approximately decadal frequency (Burgi et al. 2014; Pouclet and Bram 2021). Other examples of smaller (tens-of-meters diameter) lava lakes globally include Erebus, Erta ‘Ale (Ethiopia), and Villarrica (Chile) (Lev et al. 2019). Erebus is known for its relatively frequent and discrete Strombolian lava lake explosions, which produce intense, short-duration, bimodal infrasound pulses (Johnson et al. 2008; Witsil and Johnson, 2018). Erta ‘Ale can host two lava lakes at its

summit, which are typically not active at the same time. The northern lake (inactive) is fully encrusted with no incandescent zones. The southern lake is partially encrusted, with cold plates separated by incandescent cracks, and may circulate these plates anywhere between 7 and 70 min (depending on the lava lake’s convection and surface velocities) (Harris et al. 2005; Bouche et al. 2010). The level of Erta ‘Ale’s southern lava lake, which is deduced via MODIS (Moderate Resolution Imaging Spectroradiometer) satellite data, is explained by the growth and thinning of foam accumulated at the top of a shallow reservoir (Vergniolle and Bouche 2016). In addition, Erta ‘Ale produces continuous infrasound through a mechanism postulated as flat bubbles, where a series of small degassing pulses sourced from a bubble close to equilibrium results in continuous volcanic tremor at about 25–35 Hz. Villarrica’s lava lake displays a surface composed of cold plates not unlike Erta ‘Ale (including possible flat bubble eruption mechanisms), while its conduit geometry is similar to that of Mt. Etna’s (whose vents are sometimes narrow shaft conduits leading to a flaring crater) (Spina et al. 2014). Villarrica’s lava lake geometry is relatively simple. Its summit crater typically hosts a single relatively small-diameter lava lake situated ~ 100 m below the crater rim. This lava lake is the surface manifestation of its magma column (Witter et al. 2004; Palma et al. 2008; Moussallam et al. 2016). Villarrica’s resonant infrasound is mostly stationary and continuous, often characterized by monotonic tremors (Goto and Johnson 2011). Excursions in infrasonic frequencies have been correlated to its lava lake level (Richardson et al. 2014; Johnson et al. 2018b).

Volcán Villarrica is the most continuously active volcano of the Andes Southern Volcanic Zone and is an especially prominent and well-known radiator of infrasound (Ripepe et al. 2010; Goto and Johnson 2011). It is an open-vent, symmetric 2860-m-tall stratovolcano with persistent degassing from the nearly continuously present lava lake within its summit crater (Palma et al. 2008). Villarrica is predominantly basaltic in chemistry and formed in the Mid-to-Late Pleistocene era (~ 100 ka before the present) and has been active with a pattern of explosive prehistoric caldera collapses followed by periods of rebuilding (Dzierma and Wehrmann 2010). The historic explosive activity of Villarrica is characterized as Strombolian style with a varying intensity such that sometimes it is unsafe to visit the crater rim (Gurioli et al. 2008). Presently, Villarrica is one of Chile’s most popular tourist destinations, and guided climbs to the summit are common in the Austral summer. Since it is located in an area with high population density and tourist traffic, even small eruptions pose hazards to climbers while larger eruptions present hazards to the surrounding towns of Pucón and Villarrica (Dzierma and Wehrmann 2010). Villarrica’s glaciated summit poses a particular threat for producing lahars during approximately decadal paroxysmal

eruptions (Van Daele et al. 2014; Johnson and Palma 2015; Naranjo and Moreno 2016).

Volcán Villarrica is a reliable laboratory for volcano infrasound studies due to its active lava lake and stationary and continuous production of infrasound (Ripepe et al. 2010; Goto and Johnson 2011; Richardson and Waite 2013). Given that Villarrica is one of the most continually active volcanoes in Chile, multidisciplinary monitoring, including infrasound surveillance, is critical for proper hazard assessment. Villarrica's most recent paroxysmal eruption on 3 March 2015 was a short-lived but violent VEI 2 event (Johnson et al. 2018b; Romero et al. 2018), whose eruption was preceded by a rise in Villarrica's infrasonic frequency correlated attributed to a rise in lava lake level. With this observation indicating a possible precursor to eruptions at Villarrica, we now investigate the limits to Villarrica's infrasonic frequency fluctuations while its lava lake level remains in an unvarying background state.

Our field experiment in January 2020 was designed to record Villarrica's infrasonic frequencies close to the source using a dense network of 20 sensors. Over the week-long recording period, volcanic activity was stable and there were no changes to the crater's geometry, no noticeable change in eruption styles, and no large explosive eruptions (i.e., ejecta leaving the crater rim). Although small, approximately hourly spatter events from the lava lake were noted, the source and mechanism of Villarrica's continuous monotonic infrasound were largely unchanged compared to previous experiments with longer recording intervals (e.g., Shinohara and Witter 2005; Richardson et al. 2014; Johnson et al. 2018b). Since the frequency content of Villarrica's infrasound has been proposed as a powerful forecasting tool (Johnson et al. 2018b), we postulated that any frequency fluctuation could be relatable to either crater geometric changes (i.e., lava lake level) or changes in the nature of the volcano's activity. Given the unchanging crater shape during our study period, this work focuses on non-geometric factors, such as sound speed (i.e., temperature), infrasound source characteristics, and the spatial distribution of sensors around the crater, to better understand their impact on the observed frequency content during a stable monitoring period.

Data/methods

Infrasound

Twenty Gem infrasound loggers (Anderson et al. 2018) were installed at the summit of Villarrica between 12 and 19 January 2020 and recorded continuous infrasound using GPS time synchronization and position information. Acquisition parameters include a sample rate of 100 Hz, a

sensor sensitivity that is flat between 0.04 and 27 Hz (several octaves above and below the signals of interest), and an RMS noise floor of 3 mPa, which is lower than the background environmental noise. The Gem infrasound loggers are ideal for a week-long deployment given their low cost, compact, and lightweight packaging (~400 g plus batteries) and ease of deployment. We used three D-cells for each sensor, which can run a Gem continuously for about two months.

We broadly classify data for each sensor based upon its position ("I," "O," or "C"). Seven sensors were situated inside ("I"), and ten were located outside ("O") the crater rim and hidden away from areas frequented by tourists. Three additional sensors deployed between January 16 and January 19 were situated on a cable ("C") strung across the crater in an east/west orientation (Fig. 1). Cabled microphones were unspooled from each side using deep sea fishing reel winches.

Seventeen of the summit sensors were recorded continuously for a full week starting on 12 January 2020, while three of the cable sensors were deployed later and recorded continuously for the last three days until 19 January. In our analysis, all signals were bandpass filtered between 0.55 and 5 Hz using a fourth-order Butterworth filter. This band was chosen to reduce microbarom noise below 0.5 Hz and noise at or above 5 Hz while still capturing the frequency band of interest associated with Villarrica's activity. Historically, there does not appear to be much volcanic infrasound signal at Villarrica below the 0.55-Hz threshold (Johnson and Ripepe 2011) and above 5 Hz, where signal-to-noise ratios are low. Figure 2 compares the raw recorded signal (Fig. 2c, g) with filtered data (Fig. 2a, b, d, e, f, h) for a subset of six of twenty infrasound channels representing geographically dispersed stations {c097 (C), s012 (I), s010 (I), s084 (I), s100 (O), and s094 (O)}. These same six channels are highlighted in later figures and analyses. Data shown in Fig. 2 represents both infrasonic tremor and some discrete infrasound bursts evident in the 720-s time series (Fig. 2a).

InfraFDTD and DEM

Previous studies have used numerical modeling of acoustic waves to investigate the relationship between peak frequency and crater geometry (Fee et al. 2010; Richardson et al. 2014; Witsil and Johnson 2018; Watson et al. 2019); however, less work has focused on understanding the influence of the spatial positioning of sensors located in the vicinity of the crater. To help quantify and interpret potential frequency differences among stations, we model the site-dependent response of each location where we have deployed infrasound sensors. We use InfraFDTD, a 3D finite-difference time-domain (FDTD) acoustic wave propagation model, to quantify the influence of crater topography and atmospheric

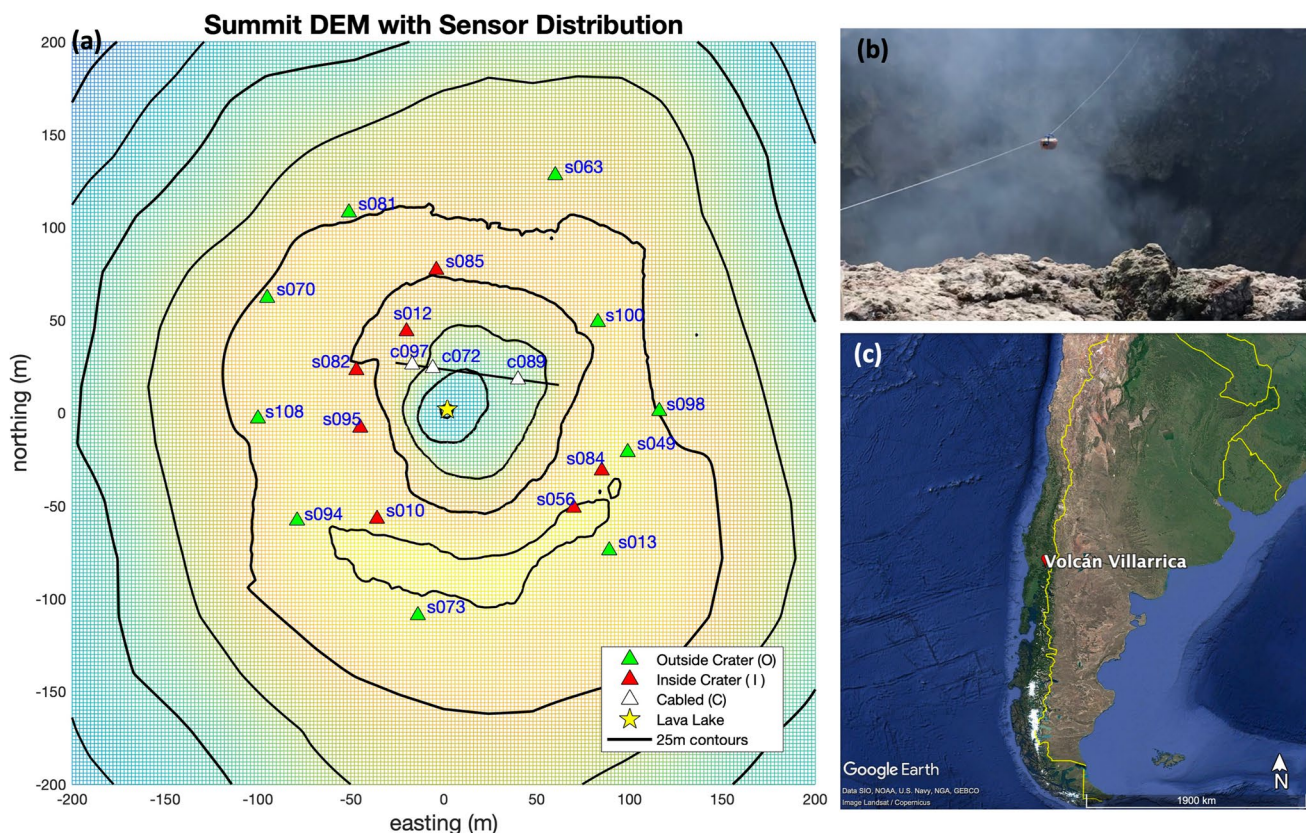


Fig. 1 (a) Contour map from digital elevation model (DEM) of Villarrica's summit showing locations of the 20 sensors and the cable. (b) Zoomed-in photo of Gem logger (c089) suspended on the cable

(seen from the northeast). (c) Locator map of Villarrica's position within South America

properties on the source-time functions. The primary input to the model is the digital elevation model (DEM) for the crater. This is derived from drone-based structure-from-motion (SfM) surveys made in mid-January, and we assume that both the DEM and the location of the lava lake at the bottom of the crater did not change over the week-long data acquisition interval. The DEM's resolution is interpolated to a 2-m grid and derived from ~ 150 images taken during an overflight using a DJI Mavic Pro quadcopter. Visibility to the bottom of the crater was unobstructed during the aerial overflights allowing for a map of the full extent of the crater.

InfraFDTD, developed by Kim and Lees (2014), implements a source that we fix at the lava lake at the bottom of the crater. The model solves the acoustic wave equation over a 3-dimensional topographic domain and is widely used in a variety of previous volcanic studies (Kim and Lees 2011; Kim et al. 2012; Lacanna and Ripepe 2013). Although the code does not accommodate an advecting (windy) atmosphere, it does allow vertically varying sound speed structures, user-specified DEMs, and user-selected source-time functions. InfraFDTD uses a perfectly matched layer absorbing boundary condition at the computational domain boundaries and a perfectly

reflecting boundary on the topographic surfaces. The perfectly reflecting boundary condition is often used for infrasound modeling in volcano settings, resulting in a successful prediction of infrasound diffraction and reflection over complex topography (Lacanna and Ripepe 2013; Kim and Lees 2014; Maher et al. 2021). The high contrast of sound speeds and densities across the solid-air boundary transmits only a small amount (< 2%) of acoustic energy to the solid earth (Bishop et al. 2022) and justifies the assumption of perfect reflection. Our model space extended to the limits of the map shown in Fig. 1a, and in our experience, the absorbing boundary condition at the edge of the model space performed well. Wavefield simulations did not show artifacts reflected off of the model boundaries.

InfraFDTD requires a GPU and makes use of a high-resolution DEM with an arbitrary topography. This modeling is more computationally intensive than 1D simulations such as Cres (crater resonance) (Watson et al. 2019), but is potentially very important for understanding the impact of topography that is not axisymmetric. Because the objective of this study is focused on spatial frequency variability, the 3D InfraFDTD model is appropriate and necessary.

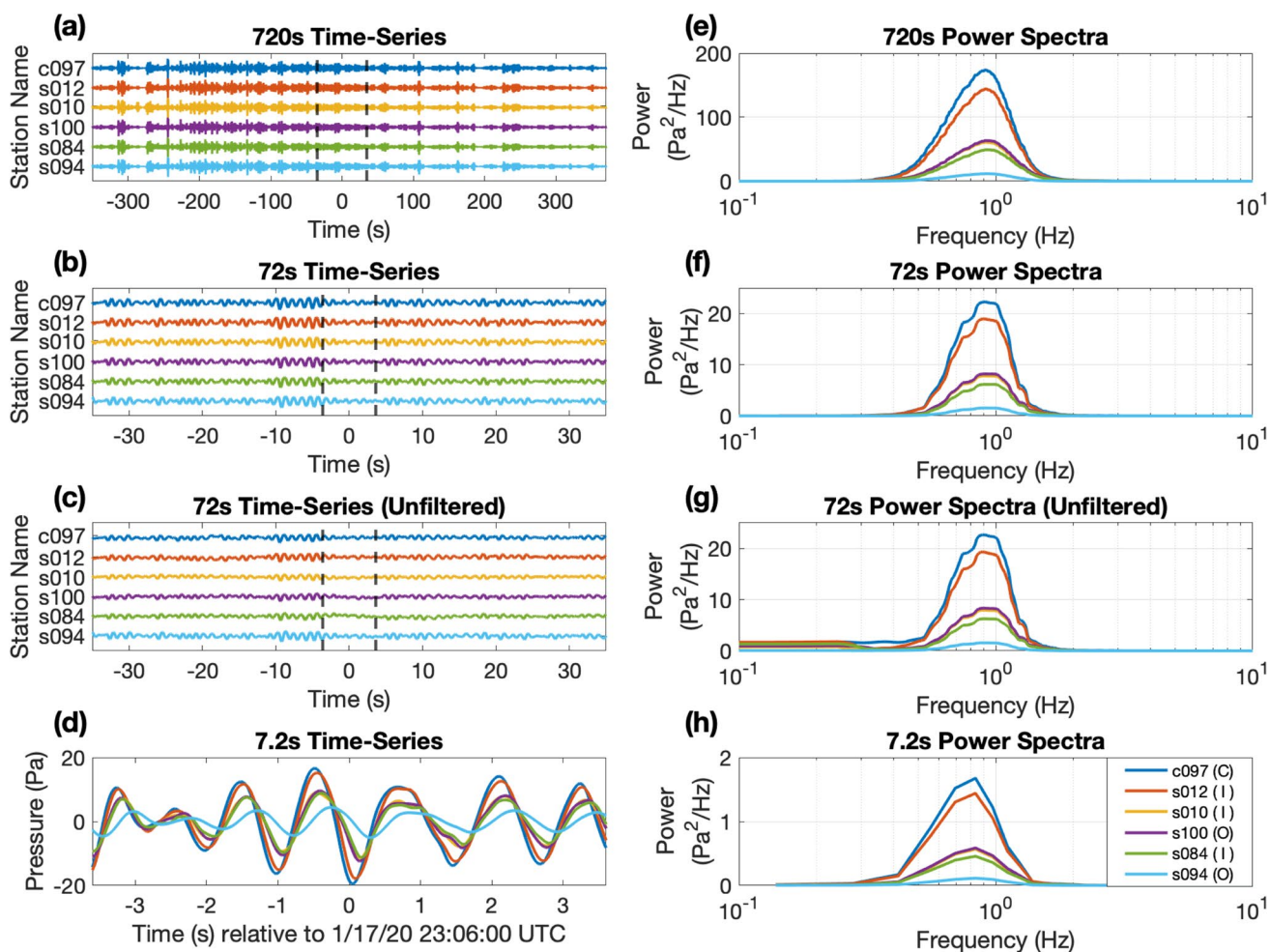


Fig. 2 Example infrasound signals from six stations deployed on the summit of Villarrica in 2020. Time-series data are bandpass filtered between 0.55 and 5 Hz except for panel (c), which is unfiltered. Power spectra are smoothed with a 0.5-Hz spectral averaging Daniell filter. (a) Normalized, 720-s waveforms contain continuous ~1 Hz infrasound (tremor) as well as three discrete events occurring

at -310 s, -250 s, and 225 s. (b) The same normalized waveforms zoomed to a 72-s window show waveform detail. (c) Unfiltered waveforms from panel (b). (d) Waveforms zoomed in to 7.2-s are overlaid and shown with amplitude scale in Pa. (e, f, g, h) Spectra are provided for waveforms in panels a, b, c, and d, respectively

Model runs are computed on a graphics processing unit (GPU) from the high-performance computer cluster R2 at Boise State, which can parallelize the FDTD calculations for fast simulations permitting many tests with varying parameters. Our standard model run, which involves $250 \times 250 \times 500$ grid nodes with 2-m spacing (corresponding to the mapped region in Fig. 1) and 2000 time-steps (corresponding to 0.0025-s intervals, 5 s total), takes about 5 min to run on the cluster. High-frequency waves can be simulated without artificial scattering and dispersion by using at least 10 points per wavelength (Wang 1996). Kim and Lees (2011) use 20 points per wavelength to suppress numerical dispersion which sets our maximum frequency at 20 Hz, suitably higher than the frequency band in question. InfraFDTD models were run many times to help understand the effect of a variety of parameters including source-time

functions and variations in a homogeneous sound speed. Synthetic waveform outputs are calculated at specific locations corresponding to sensor deployment positions (see Fig. 1).

Source-time functions at the lava lake surface are provided as mass flux time-series input and are provided with different frequency contents to compute Villarrica's transfer function or acoustic crater response (as termed by Johnson et al. (2018b) and Watson et al. (2020)). Our source inputs include Blackman-Harris functions (Harris 1978) ranging from 0.7 to 2.5 Hz as well as a bandpass filtered (0.55–5 Hz) impulse, which is more broadband. Blackman-Harris acoustic source functions are convenient, band-limited, short-duration time-series signals (Kim and Lees 2011; 2014), which have been used in previous studies to model discrete gas emissions with finite-time

durations (McKee et al. 2017; Iezzi et al. 2019; Yokoo et al. 2019; Fee et al. 2021). The specified corner frequency of the Blackman-Harris represents the high-cut corner and may be raised/lowered to decrease/increase the time duration of the source pulse. Figure 3 shows examples of Blackman-Harris functions of 1.5 Hz and 2.5 Hz frequencies and synthetic waveform outputs for atmospheric sound speeds fixed at 350 m/s.

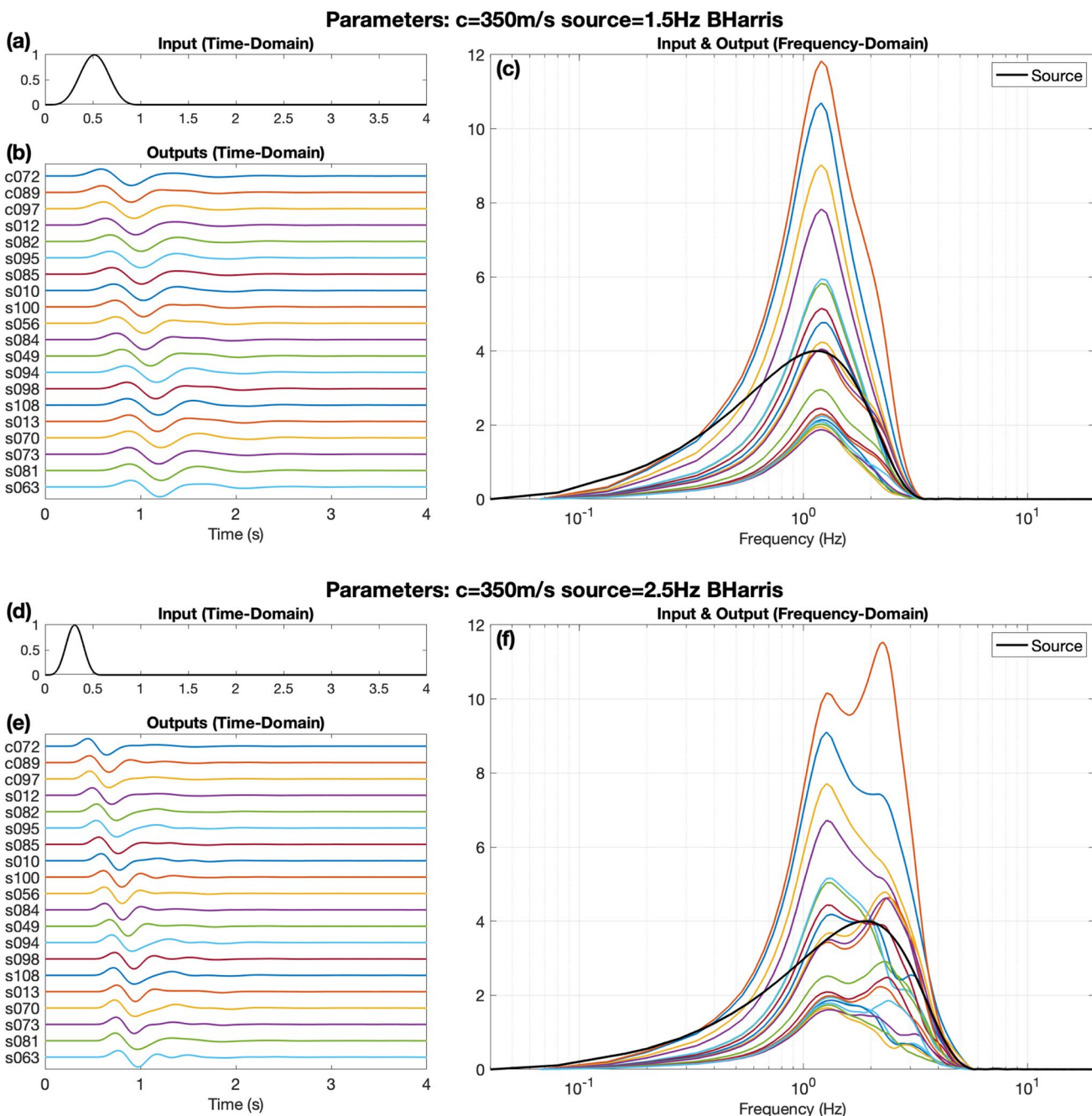


Fig. 3 Examples of two model runs with 350 m/s sound speed and normalized Blackman-Harris mass flux (kg/s) source function (a) at 1.5 Hz and (d) at 2.5 Hz. (b, e) Normalized synthetic signals at

Spectral analysis of recorded data

To quantify the peak spectral distribution of Villarrica's infrasound recorded at the summit, histograms of peak frequencies were calculated for each station for a full-day recording period. Peak frequencies are calculated from filtered data with 100 s (10,000 samples) Hamming windows and 50% overlap (see Fig. 4). Histograms of measured peak frequencies are Gaussian shaped for

the sensor positions are shown as receiver gathers. (c, f) Spectra of synthetic signals (Pa) for all stations are given along with the source input frequency spectrum (black curve)

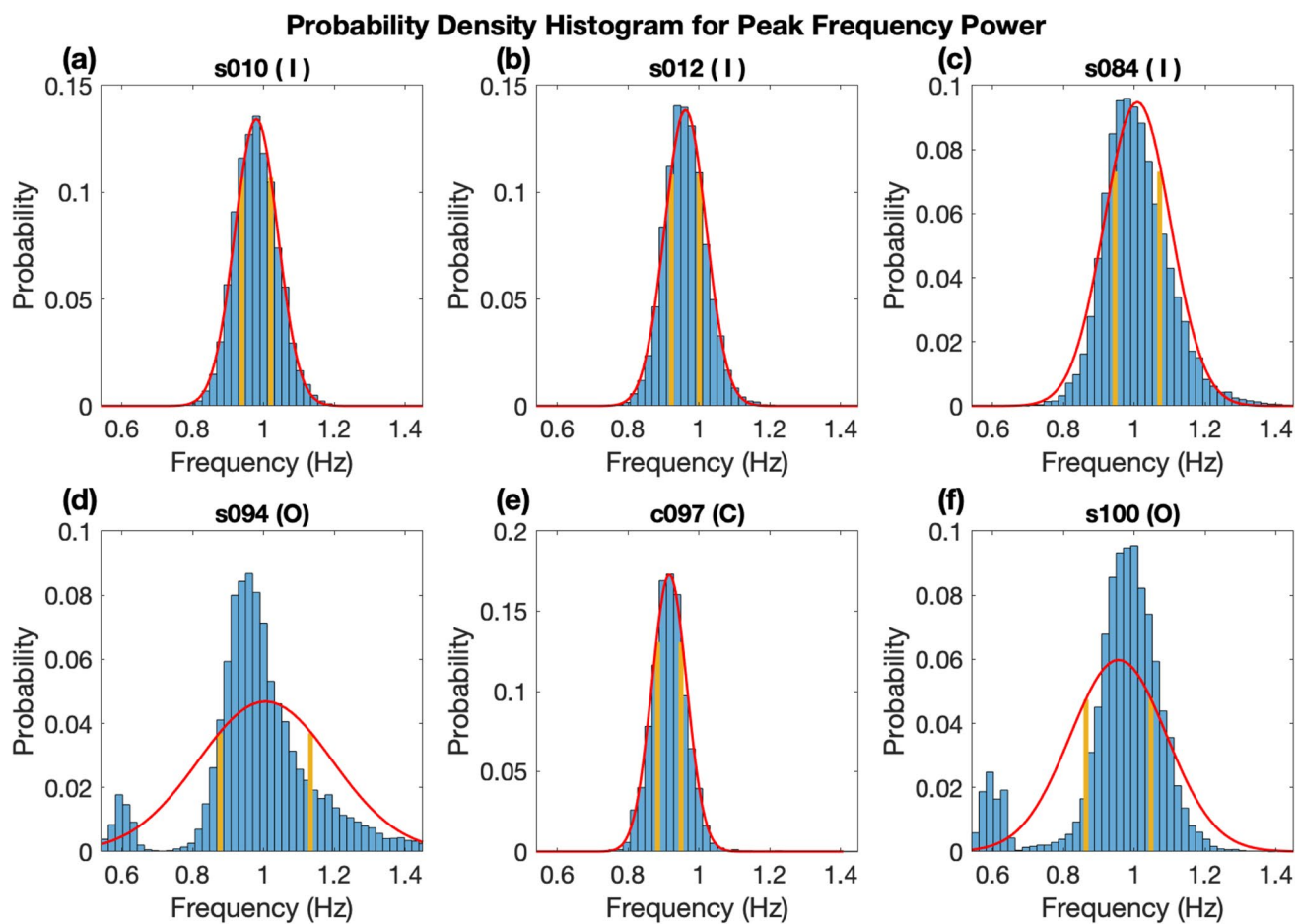


Fig. 4 (a–f) Day-long probability mass functions of peak frequencies for six different stations and best-fit normal distribution showing 25th and 75th percentiles. Peak frequencies are calculated with 100 s windows and 50% overlap, resulting in ~1700 windows grouped into 50 bins

stations located within the crater and on the cable (e.g., s010, s012, s084, c097), whereas s094 and s100 (on, or outside, the crater rim) show an occasional second peak frequency at ~0.5 Hz presumably associated with time windows when microbarom peaks were more pronounced than volcanic tremor peaks, i.e., when signal-to-noise outside the crater is lower. The Gaussian-shaped peak frequency distribution curves for stations inside the crater are associated with Villarrica's monotonic infrasound signal during a background state of low-level activity. The volcano's resonant frequency appears to deviate symmetrically around a central, resonant peak frequency in a normal distribution. Sensors outside the crater show deviation from the normal distribution due to the influence of microbarom contamination.

Results

Data recorded by the network show both temporal and spatial variations in peak frequency, although more variation is observed temporally. In other words, spectral peak values appear to reflect source controls as opposed to

propagation controls. For a given station, temporal variations in peak frequency have been found to vary by up to $+/- 17\%$ (e.g., 0.8 to 1.2 Hz; Fig. 4, Fig. 5), whereas spatial frequency variations across stations are more limited and deviate by only about $+/- 10\%$ (e.g., $+/- 0.1$ Hz; Fig. 6, Fig. 7a). These temporal and spatial variations are shown clearly in Fig. 7a, such as at time 350–400 s, where the mean peak frequency values shift up ~ 0.15 Hz ($+ \sim 17\%$) and the total spatial variability ranges by only ~ 0.05 Hz ($+/- \sim 3\%$). There are a few exceptions to this trend, such as at times 550 or 900 s, where the signal-to-noise ratio decreases, and ambient noise overpowers a lower amplitude tremor (Fig. 7b). This observation implies that an infrasound recording made almost anywhere at the top of Villarrica (inside or outside the crater) will reliably detect temporal changes of tremor frequency characteristics.

We explore whether a diurnal temperature cycle could influence the frequency distributions by computing frequency statistics for daytime and nighttime windows (Fig. 8). Supposing that temperatures in the crater drop

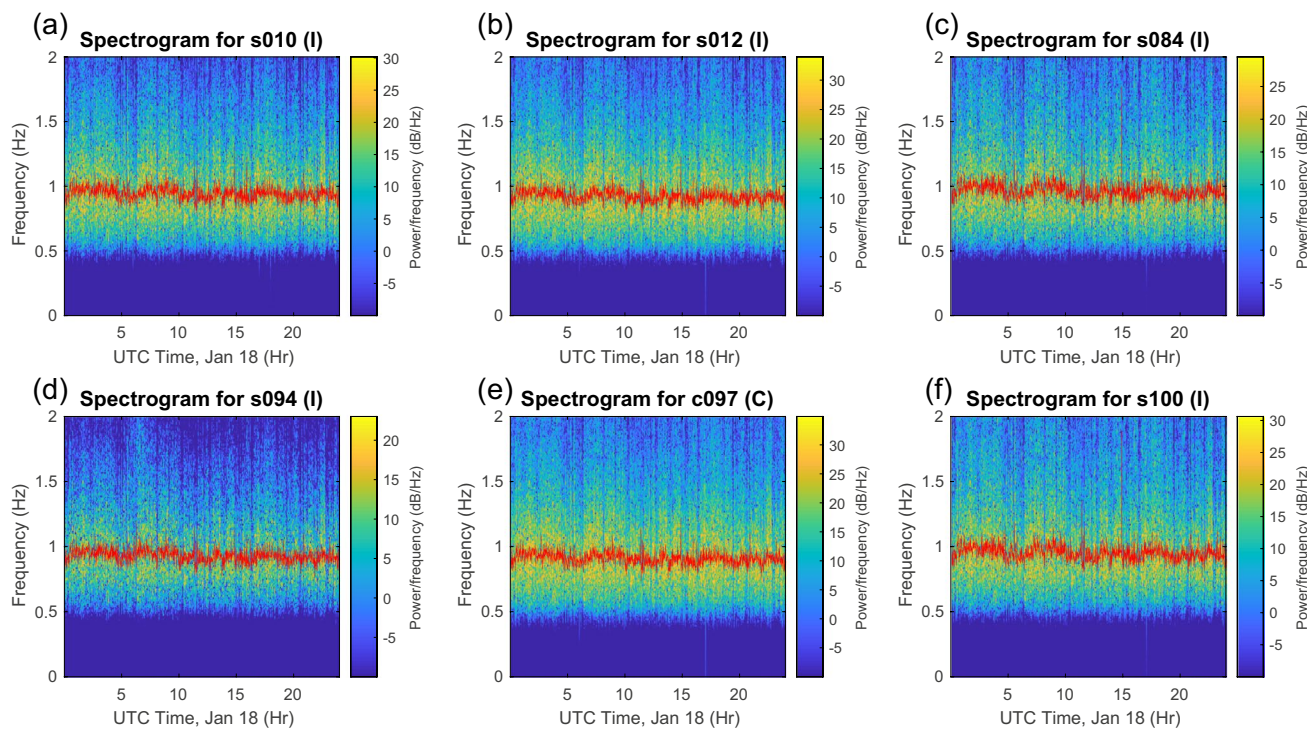


Fig. 5 (a–f) Day-long spectrograms from 18 January 2020 for the 6 stations indicated in Fig. 2. The peak amplitude frequency is shown with a red line. Window duration is 100 s with 50% overlap. Spectral content has been filtered above a 0.55-Hz corner

Fig. 6 Scatter plot comparing the peak frequencies recorded at station s010 (I) with station s100 (O). The dashed black line indicates a slope of one

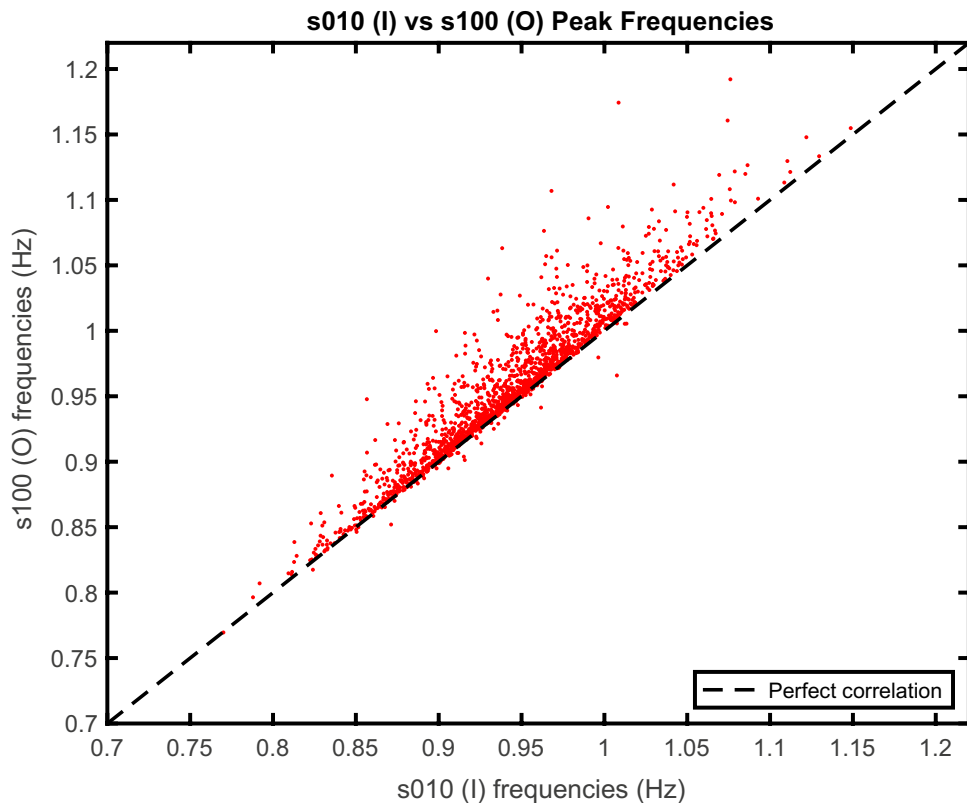
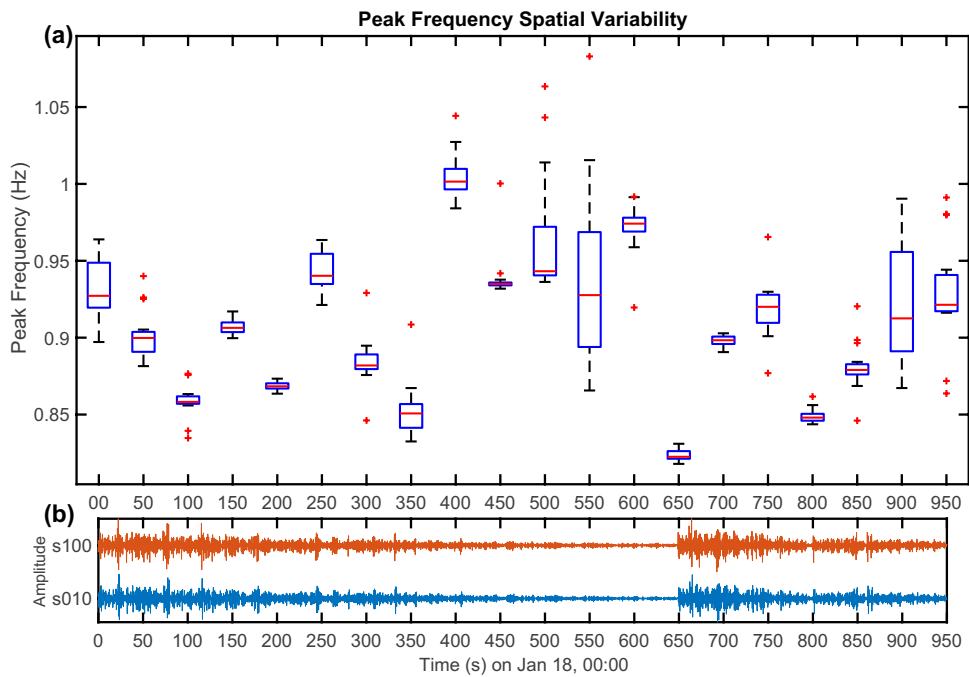


Fig. 7 (a) Box-and-whisker plots of peak frequency calculated from all 20 sensors during 20 sliding time windows of 100 s duration and within 50% overlap. Box limits correspond to 25th and 75th percentiles and whiskers extend to the maximum and minimum frequency values of all sensors except outliers. Outlier values, defined as 1.5 times the interquartile range, are indicated with red + symbols. (b) The corresponding time-series record (bandpass filtered between 0.55 and 5 Hz) are from s010 (orange; I) and s100 (blue; O) and show variations in infrasound tremor amplitude



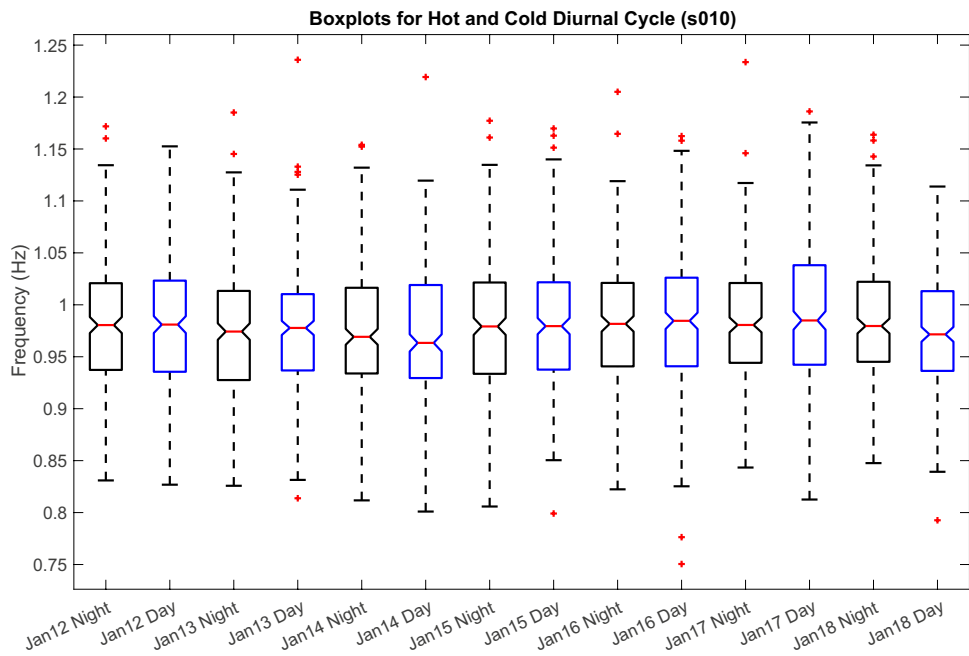
significantly at night, we might expect lower frequencies after sunset. Because no apparent day-to-night variations are detected, we discount ambient temperature variations as a primary explanation for frequency excursions.

Synthetic waveform spectra calculated by InfraFDTD are compared with recorded infrasound spectra to elucidate the source spectrum of infrasound produced by Villarrica, assuming a source affixed to the lava lake at the bottom of the crater. InfraFDTD models were run with an assortment of Blackman-Harris source-time functions (of varying

frequencies) in an attempt to forward-match a source spectrum's synthetic output to observed data. At this point, only the spectral components are investigated, and there are no attempts to invert for amplitudes of source functions.

Models are run with a range of homogeneous sound speeds using various Blackman-Harris wavelets. The InfraFDTD model produces multiple synthetic pressure time series for which peak spectral frequency is calculated. Synthetic spectra are affected both by the acoustic response of the crater (determined by sound speed and topography) and by the source function. Figure 9

Fig. 8 Box-and-whisker peak frequency plot for s010 (O) during the four coldest hours of the night (0:00–4:00, local time, black) and the four hottest hours of the day (11:00–15:00, local time, blue) for the week-long dataset. Statistics presented are in the same form as for Fig. 7. Peak frequencies are calculated from the spectrograms using 100 s windows and 50% overlap



shows trends relating Blackman-Harris source frequency and sound speed to peak output frequency. For example, using a given output frequency of 1.0 Hz, the input corner of the Blackman-Harris source wavelet needs to be 0.9 Hz at 400 m/s, 0.975 Hz at 350 m/s, and 1.3 Hz at 300 m/s sound speed. Generally, the output frequency increases as the Blackman-Harris source frequency increases up to about 1.5 Hz. Then the modeled output tends to level off, suggesting a preference for an acoustic mode at certain frequencies (less than ~1.4 Hz). This helps to explain the predominance of ~1-Hz tremor, which is a primary feature of Villarrica's infrasound.

A primary input to the model is the non-advection adiabatic sound speed, which is a function of molar mass and temperature (Pierce 2019), i.e., $c = \sqrt{\frac{\gamma RT}{M}}$ (Finn 1964). We assume in our modeling that the crater is primarily composed of a standard atmosphere (~78% N_2 and ~21% O_2), following Shinohara and Witter (2005) who reported that each plume ejection at Villarrica, which was made up of up to 95% H_2O and much lower concentrations of CO_2 and sulfur species, accounted cumulatively for only 1% of the total crater atmosphere. This low percentage of magmatic gas is supported by qualitative observations made during our field campaign, where clear visibility into and across the crater suggested a relatively low concentration of volcanic gasses. We thus use a standard molar mass for an atmosphere where the universal gas constant (R) = ~8.314 J/(mol · K) (dry air), the specific heat ratio (γ) = 1.4, and molar mass (M) = 28.95 g/mol. Even considering a 5% water vapor concentration within the crater, the molar mass would only

change by about 1%, which is much less than the variability caused by minor temperature changes.

Since we assume the crater's sound speed is principally a function of only temperature (i.e., $c = \sim 20.1 \sqrt{T}$; T is the temperature in kelvins), we attempt to characterize Villarrica's crater temperature profile using a combination of values used previously and constrained by the internal sensor temperature data provided by the Gem loggers. The Gem's internal temperature sensors, including those suspended on the cable less than 100 m above the lava lake, ranged from 4 to 28 °C during our field campaign. This corresponds to sound speeds ranging from 330 to 350 m/s at and around the crater's rim. Goto and Johnson (2011) also estimated relatively low temperatures. They speculated that the buoyant air in the crater might have occasionally reached ~50 °C owing to slightly melted plastic enclosures suspended for many hours on cables. Although spatial temperature distribution within Villarrica's crater is certainly variable and likely increases toward the crater floor, Watson et al. (2019) showed the limited impact of a moderate temperature stratigraphy. That is, model output from a homogeneous velocity model approximates a linear gradient model possessing the same average velocity.

Discussion

Because the peak frequency values for most of the recorded infrasound range between 0.8 and 1.2 Hz, our modeling indicates that the primary infrasound source probably contains

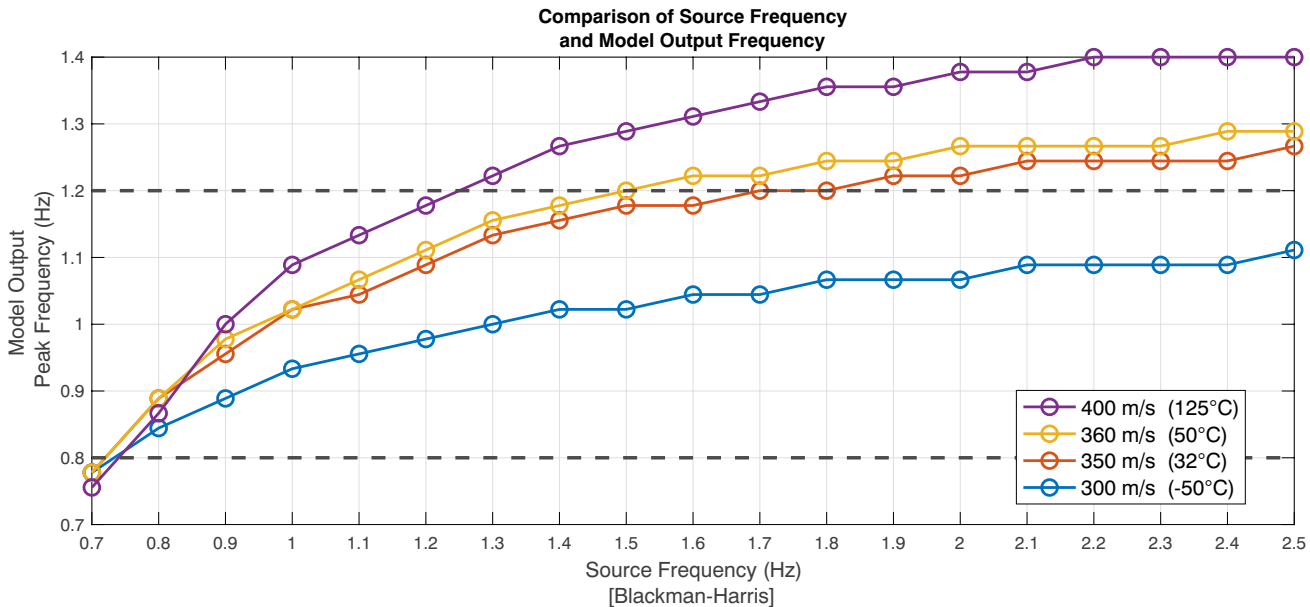


Fig. 9 Relationship between input Blackman-Harris source frequency (x -axis) and modeled peak frequency (y -axis) for a range of crater sound speeds. All model runs are calculated using a Blackman-Harris

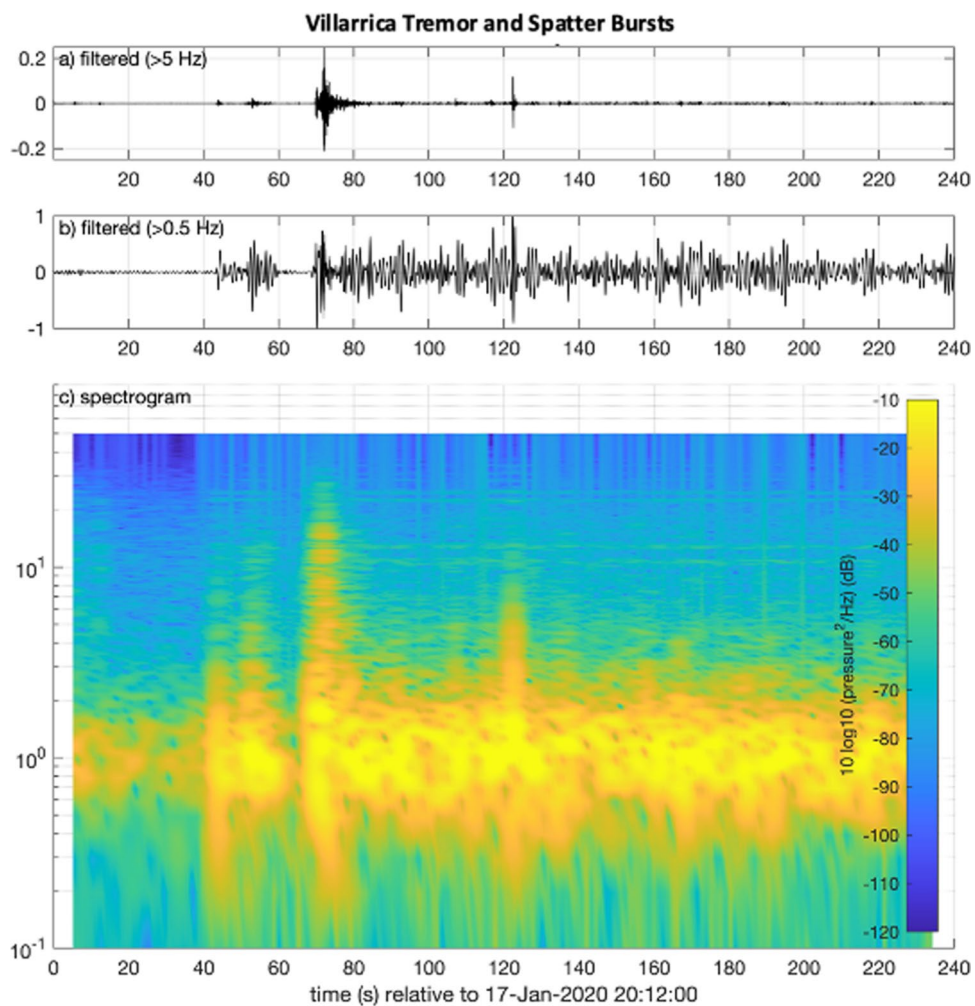
source function as an input. Dashed horizontal lines correspond to the range of peak frequencies recorded

much of its energy below 1.4 Hz (Fig. 9). Higher frequency Blackman-Harris sources can yield observed data peaked between 0.8 and 1.2 Hz only if unrealistically low sound speeds are used (e.g., 300 m/s corresponding to -50°C). This finding indicates that even though recorded infrasound is modulated by the acoustic crater response, the source must still have a predominance of low frequencies.

For reasonable crater sound speeds exceeding 350 m/s ($>\sim 30^{\circ}\text{C}$), the excursions in frequency content may be easily explained by subtle source frequency variations rather than by variations in temperature caused by diurnal cycles (see negative result from Fig. 8) or by emission of hot gas filling or partially filling the crater. We do not possess data to show how lava lake degassing perturbs the average temperature within the crater; however, given the relatively low level and stationary nature of the activity, we speculate that the average crater temperature and sound speed does not exceed 50°C (360 m/s). The observed peak frequency variations ranging $+\/-0.2$ Hz are thus most easily attributable to source variations.

We contend that the persistent lava lake degassing and/or surface convection, coupled with Villarrica's unique crater acoustic response, is responsible for the bulk of the 0.8- to 1.2-Hz tremor that has been noted in this and many previous studies over the years (Ripepe et al. 2010; Goto and Johnson 2011; Richardson and Waite 2013; Richardson et al. 2014; Johnson et al. 2018b; Watson et al. 2019). We speculate that the mechanism for this persistent degassing may be similar to what has been found at Erta 'Ale, with low, over-pressurized flat bubbles rising to the surface and roiling the lava lake/free surface interface (Bouche et al. 2010). During our 2020 fieldwork, which included camera and drone observations of the lava lake, we also noted rare and sporadic small explosion events. These spatter bursts, or small Strombolian eruptions, occurred approximately hourly and triggered infrasound transients, whose energy peaked at or above about 5 Hz. These events are evident on spectrograms with short windows (Fig. 10), in which energy above 5 Hz is evident on the recordings at all summit infrasound stations.

Fig. 10 Station s108 infrasound time series and spectrogram associated with three small spattering/Strombolian events. (a) A 5-Hz high-pass-filtered time series shows events with energy above 5 Hz. (b) A 0.5-Hz high-pass-filtered time series shows the prevalent background tremor with the high-frequency components largely obscured. (c) Spectrogram of the 0.5-Hz high-passed data are calculated for 10 s intervals and 50% window overlap



The small Strombolian eruptions at Villarrica begin suddenly and are impulsive in their infrasound signature with a corresponding signal spectrum that is relatively broadband. Although not predictable, they occasionally followed periods in which the pervasive background tremor was temporarily absent (see, for example, the first two pulses in Fig. 10). The interplay of discrete explosions with tremor suggests that the supply of volatiles to the top of the magma column may occasionally be impeded by a shallow high-viscosity layer (Davaille and Jaupart 1993; Lev et al. 2019). We suspect that volatiles might collect in the upper conduit for a period of a few tens of seconds before exploding and upsetting the viscosity stratification.

Low-frequency Blackman-Harris functions do not produce synthetic signals with energy above ~ 5 Hz, so we attempt to replicate the recorded data using a broadband source composed of an impulse delta function band passed between 0.55 and 5 Hz (Fig. 11). This broadband source produces synthetic spectra, which have odd overtones (i.e., peaks at 3 and 5 times the fundamental frequency; ~ 3 Hz and ~ 5 Hz). These odd integer modes suggest open-closed pipe resonance, where one end of a tubular cavity is restricted, and only odd integers of the fundamental frequency can be sustained. This open-closed volcanic pipe analog has been suggested by others where odd overtones are present (Fig. 2 in Johnson et al. 2018a). The peak frequency spectra at Cotopaxi and some craters at Mt. Etna

(Spina et al. 2014) have a dominant amplitude at the fundamental frequency, as opposed to the situation at Villarrica, where the overtones appear to have higher amplitudes. These differences can be due to crater shape geometry, which was shaft-like at Cotopaxi and Mt. Etna compared to a funnel shape at Villarrica. They can also be due to differences in source excitation. Villarrica's spatter bursts likely contain a predominance of high frequencies, given their short duration and impulsive nature.

We have identified two types of sources at Villarrica, which have different infrasound signatures (Fig. 12). In 2020, Villarrica's Strombolian eruptions were much smaller than the lower frequency 0.7–1 Hz explosions described by Johnson et al. (2018b) leading up to the 3 March 2015 paroxysm. Those presumably larger explosions were effective at exciting the lower frequency resonant modes of a ~ 100 -m deep crater. Based on the depth of Villarrica's crater and the frequency of the continuous infrasound, we assume that the continuous monotonic infrasound is indicative of a fundamental acoustic resonance for Villarrica's crater controlled by the dimension of the crater down to the lava lake-free surface. The small spatter bursts in 2020 did not easily excite the fundamental frequency but had enough high-frequency energy to excite the higher modes. Notably, the 2015 eruption sequence was only recorded by infrasound sensors 4 km (and further) from the summit such that higher frequency infrasound, if present at the source, might have been attenuated through propagation.

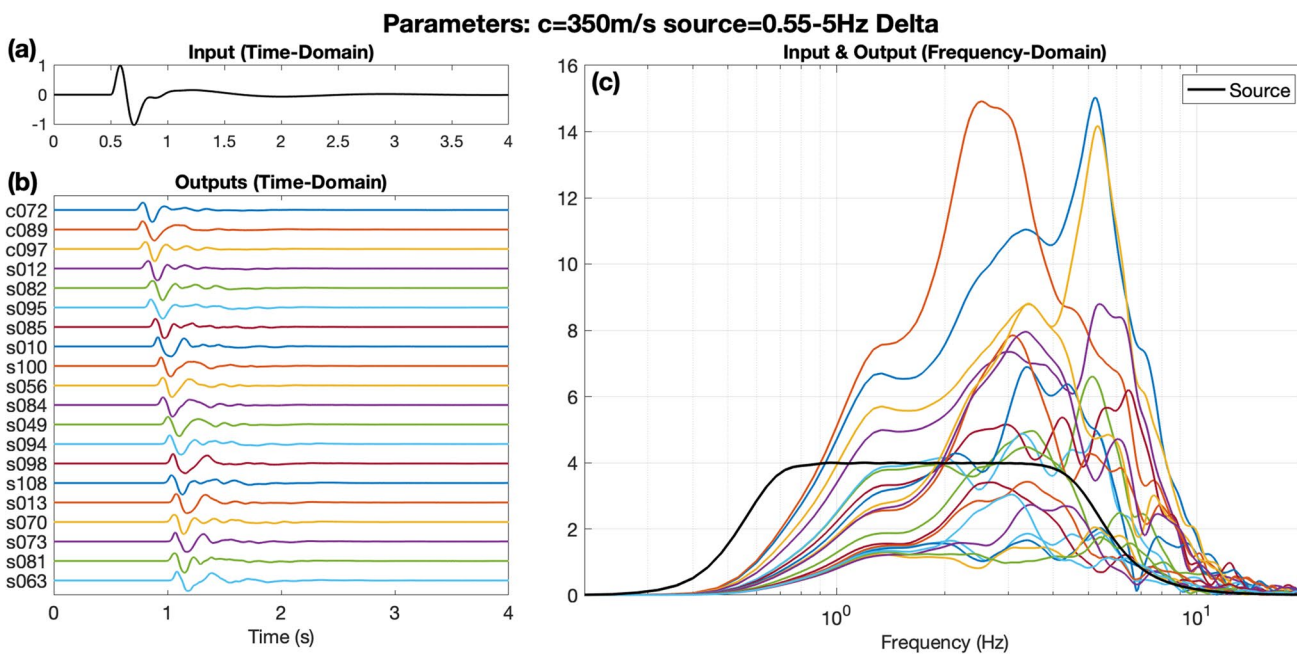


Fig. 11 Impulse source-time function and modeled time series and spectra using a 350 m/s homogeneous sound speed. (a) Modeled Dirac delta function is bandpass filtered with 4 poles between 0.55 and 5 Hz and represents normalized mass flux rate (kg/s). (b) Syn-

thetic time-series output is shown for the distributions of sensors deployed at Villarrica. (c) Output amplitude spectra are shown along with the black curve, which indicates the source-time function spectrum

To quantify the source spectrum of Villarrica's continuous infrasound tremor and test whether source inversion is similar using various stations, we attempt to deconvolve the synthetically derived Green's functions in the frequency domain. Using the impulse response highlighted in Fig. 11, we calculate a source spectrum valid specifically within the frequency range of 0.55 to 5 Hz assuming a time-invariant linear Green's function (Riad 1986). Source spectra solutions are calculated for each station by dividing the recorded tremor spectrum by the synthetic Green's function for each respective station (Fig. 13).

The inverted source spectra in Fig. 13b have similar shapes and amplitudes, which vary by about 25% (e.g., s100 compared with s094 in Fig. 11b). The amplitude differences are small but may be attributed to errors in the DEM model, the assumption in InfraFDTD of a perfectly reflecting solid/air boundary, the assumption of precise source location at the middle of the crater

bottom, and/or accuracy of GPS-located sensors. Additionally, wind and/or buoyant plume-adverted atmosphere is not integrated into InfraFDTD and may potentially be a source of the discrepancy. Nevertheless, this consistent source spectral shape indicates the spectral properties of the source-time function.

Limitations

We highlight a few limitations of the presented study to provide potential direction for future work. To begin, we wish that we had made temperature or gas composition measurements during the time of infrasound collection. This data would have been beneficial for finding more direct sound speeds within the crater as it varies over both time and space. Another limitation of this study was the absence of a video record of Villarrica's lava lake level activity during the collection period. Since the

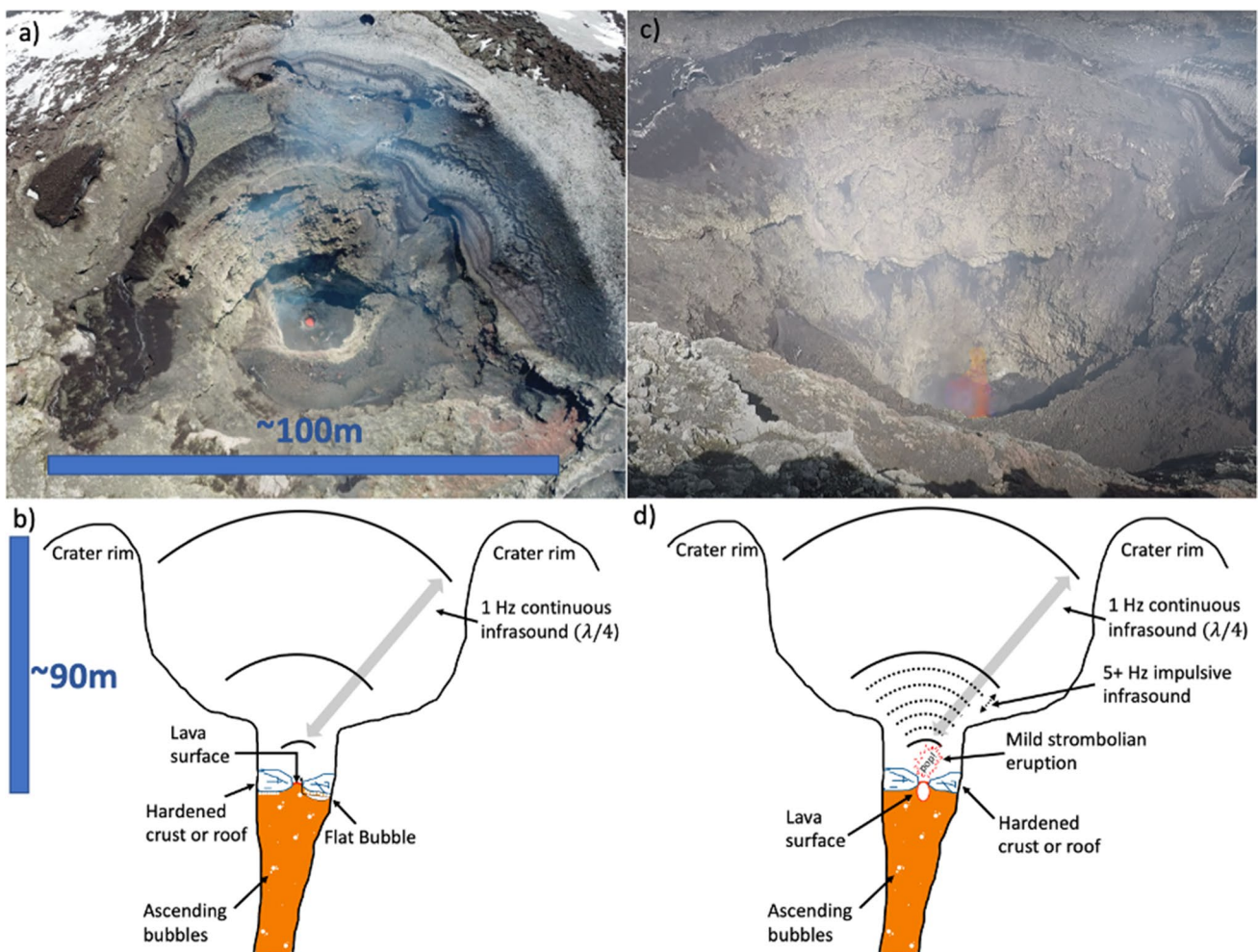


Fig. 12 Photos of Villarrica's crater and schematic interpretation of geometry and sound wavelengths. (a) UAV-based photograph of the inside of Villarrica's crater taken on 15 January 2020 shows a partially crusted-over lava lake. (b) The schematic cross-section of the crater highlights the continuous, 1-Hz infrasound standing wavefronts

drawn to approximate scale. (c) Photograph taken from the crater rim captures a small Strombolian eruption on 16 January 2020. (d) Schematic cross-section of the crater during Strombolian activity shows impulsive 5-Hz infrasound wavelengths drawn approximately to scale

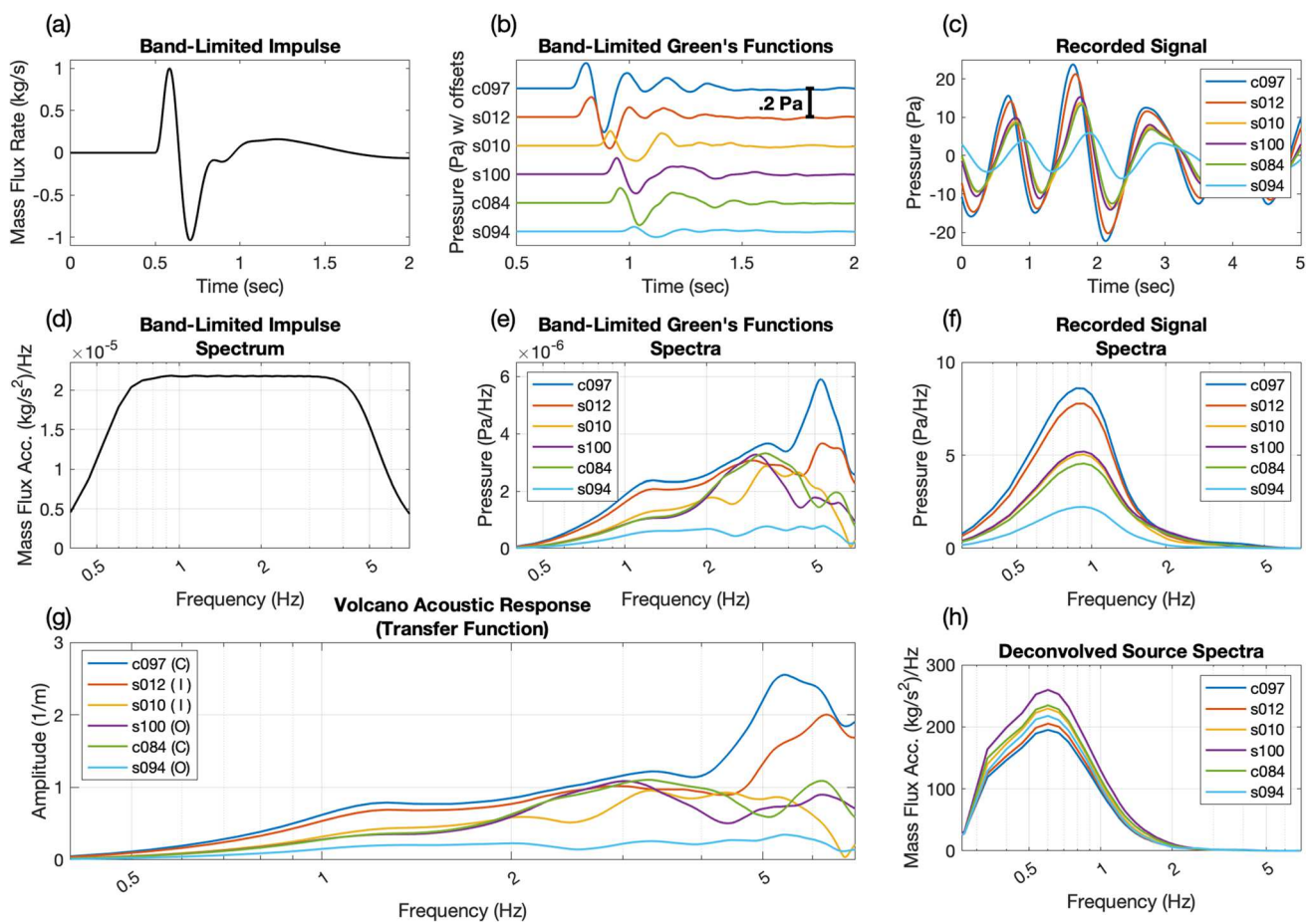


Fig. 13 Workflow for the band-limited deconvolution of crater acoustic response from tremor examples at 6 stations. **(a)** Band-limited impulse from Fig. 11a is used to calculate **(b)** the band-limited Green's functions. **(c)** Tremor data represents examples recorded at several stations from 18 January. **(d, e, f)** Frequency spectra are

shown for panels **a**, **b**, and **c**, respectively. **(g)** Transfer function, or volcano crater acoustic response, calculated as the band-limited Green's functions' spectra divided by the source impulse spectrum. **(h)** Deconvolved source spectra calculated from the recorded signal spectrum (panel **f**) divided by the crater acoustic response (panel **g**)

lava lake level was quite low during the experiment, it could not be observed from the crater rim. In future work, we advocate for deploying a gimbaled camera looking down from the suspended cable and/or making longer-duration GPS-synced drone video observations of lava lake activity. Lastly, this study only spanned a week's record of activity for which infrasound data was collected. While this was appropriate for the methods and analyses presented herein, we did not observe longer-term frequency excursions of Villarrica's tremor, such as those described by Richardson et al. (2014), that would be possibly associated with dynamic changes in the lava lake.

Conclusion

Villarrica is a classic example of an open-vent volcano producing continuous infrasonic tremor with a peaked spectrum. This infrasound tremor appears to be sourced by

an actively convecting lava lake deep within a resonating horn-shaped crater. The spectrum of Villarrica's infrasound has previously been shown to be a useful indicator of lava lake level (Johnson et al. 2018a, b), and our experiment was designed to understand the infrasound tremor during a period of relative quiescence. To help assess what constitutes a meaningful change in Villarrica's spectrum, we were able to examine ordinary fluctuations in Villarrica's infrasound spectrum during a period of low activity. Our study quantifies the dominant spectral peak at Villarrica and its variability over both time and space using a network of twenty infrasonic microphones around and within the crater rim, including three suspended over the lava lake on a cable. Signals recorded continuously over one week in January 2020 showed that a low-frequency 1-Hz tremor exhibited excursions of up to $+/- 0.2$ Hz ($+/- 17\%$) and that it was observed across the crater network. Since a rise in Villarrica's frequency content may be a precursor to future

paroxysms, the variability of this frequency, which appears to be a source effect rather than a path effect, is of importance for monitoring and forecasting future eruptions.

This study has also identified two independent sources for Villarrica's infrasound including the continuous ~1-Hz tremor as well as discrete bursts. The continuous signal is resonant in nature with a peaked spectrum, while the discrete signal involves a more broadband signal that is relatively short-lived. Results from the InfraFDTD model explain the spectral content of the two sources, which both occur at the bottom of the crater at the free surface of the lava lake. Our study spanned a one-week period in January 2020, but we suggest it could be useful to investigate other periods when Villarrica might be in a different background state and when the lava lake might be at a different level. While the ability to assess the height of Villarrica's lava lake level via tremor may be somewhat unique to this system alone, replicating our deployment (i.e., using a dense distribution of portable, self-contained Gem infrasound loggers (Anderson et al. 2018) near the source) at other open-vent volcanoes such as Nyiragongo, Halema'uma'u, Erta 'Ale, Erebus, Yasur, or Santiaguito, or volcanoes with a similar shape, such as Mt. Etna, could be an effective means to characterize near-source spatial and temporal frequency excursions. It would be useful to quantify background activity at many open-vent volcanoes such that infrasound monitoring can be implemented more effectively during future periods of unrest.

Acknowledgements The authors are grateful to anonymous reviewers who provided useful and constructive feedback. We also appreciate individuals who helped in the acquisition of the infrasound data including Jerry Mock, Kate Bollen, and Leighton Watson. This work would not have been possible without assistance from Pucón guide Ruben Paillelef, other Villarrica climbing guides, SERNAGEOMIN (Temuco), and povi.cl (Pucón). This work was partially supported by the National Science Foundation Grant EAR-1830976.

Funding This work was partially supported by the National Science Foundation Grant EAR-1830976.

Data availability Data presented here are archived and may be downloaded from the Incorporated Research Institutions for Seismology (IRIS) Data Management Center (DMC). Data may also be accessed in MATLAB format from the Boise State University Infrasound Data Repository at https://scholarworks.boisestate.edu/infrasound_data/ and doi:10.18122/infrasound_data.8.boisestate.

Data management plan Infrasound data used in this study are available at the Boise State University Infrasound Data Repository (https://scholarworks.boisestate.edu/infrasound_data/8/)

Code availability No code available.

Declarations

Ethics approval No ethics are in question for this study.

Consent to participate All authors and co-authors have given their consent to be included in this manuscript.

Consent for publication Consent has been given for publishing this manuscript.

Conflict of interest The authors declare no competing interests.

References

Lamb O, Lees J, Marin L F, Lazo J, Rivera A, Shore M, Lee S (2020) Identifying icequakes at ice-covered volcanoes in Southern Chile. EGU General Assembly 2020, Online, 4–8 May 2020, EGU2020-851. [10.5194/egusphere-egu2020-851](https://doi.org/10.5194/egusphere-egu2020-851)

Allstadt KE, Matoza RS, Lockhart AB, Moran SC, Caplan-Auerbach J, Haney MM, Thelen WA, Malone SD (2018) Seismic and acoustic signatures of surficial mass movements at volcanoes. *J Volcanol Geoth Res* 364:76–106. <https://doi.org/10.1016/j.jvolgeores.2018.09.007>

Anderson JF, Johnson JB, Bowman DC, Ronan TJ (2018) The Gem infrasound logger and custom-built instrumentation. *Seismol Res Lett* 89(1):153–164. <https://doi.org/10.1785/0220170067>

Barrière J, D'Oreye N, Oth A, Geirsson H, Mashagiro N, Johnson J B, Smets B, Samsonov S, Kervyn F (2018) Single-station seismo-acoustic monitoring of Nyiragongo's lava lake activity (D.R. Congo). *Front Earth Sci* 6(6):1–17. <https://doi.org/10.3389/feart.2018.00082>

Bishop J W, Fee D, Modrak R, Tape C, Kim K (2022) Spectral element modeling of acoustic to seismic coupling over topography. *Journal of Geophysical Research: Solid Earth* 127(1). <https://doi.org/10.1029/2021JB023142>

Bouche E, Vergniolle S, Staudacher T, Nercessian A, Delmont JC, Frogneux M, Cartault F, Le Pichon A (2010) The role of large bubbles detected from acoustic measurements on the dynamics of Erta 'Ale lava lake (Ethiopia). *Earth Planet Sci Lett* 295(1–2):37–48. <https://doi.org/10.1016/j.epsl.2010.03.020>

Burgi PY, Darrah TH, Tedesco D, Eymold WK (2014) Dynamics of the Mount Nyiragongo lava lake. *Journal of Geophysical Research: Solid Earth* 119(5):4106–4122. <https://doi.org/10.1002/2013JB010895>

Caplan-Auerbach J, Bellesiles A, Fernandes JK (2010) Estimates of eruption velocity and plume height from infrasonic recordings of the 2006 eruption of Augustine Volcano, Alaska. *J Volcanol Geotherm Res* 189:12–18. <https://doi.org/10.1016/j.jvolgeores.2009.10.002>

Davaille A, Jaupart C (1993) Thermal convection in lava lakes. *Geophys Res Lett* 20(17):1827–1830. <https://doi.org/10.1029/93GL02008>

Dzierma Y, Wehrmann H (2010) Eruption time series statistically examined: probabilities of future eruptions at Villarrica and Llaima Volcanoes, Southern Volcanic Zone, Chile. *J Volcanol Geoth Res* 193(1–2):82–92. <https://doi.org/10.1016/j.jvolgeores.2010.03.009>

Fee D, Garcés M, Patrick M, Chouet B, Dawson P, Swanson D (2010) Infrasonic harmonic tremor and degassing bursts from Halema'uma'u Crater, Kilauea Volcano. *Hawaii Journal of Geophysical Research: Solid Earth* 115(11):1–15. <https://doi.org/10.1029/2010JB007642>

Fee D, Toney L, Kim K, Sanderson RW, Iezzi AM, Matoza RS, De Angelis S, Jolly AD, Lyons JJ, Haney MM (2021) Local explosion detection and infrasound localization by reverse time migration using 3-D finite-difference wave propagation. *Front Earth Sci* 9(2):1–14. <https://doi.org/10.3389/feart.2021.620813>

Finn BS (1964) Laplace and the speed of sound. *Isis* 55(1):7–19. <https://doi.org/10.1086/349791>

Global Volcanism Program (2020) Report on Villarrica (Chile). In: Sennert, S K (ed.), *Weekly Volcanic Activity Report*, 22

January–28 January 2020. Smithsonian Institution and US Geological Survey.

Goto A, Johnson JB (2011) Monotonic infrasound and Helmholtz resonance at Volcan Villarrica (Chile). *Geophys Res Lett* 38(6):1–5. <https://doi.org/10.1029/2011GL046858>

Gurioli L, Harris AJL, Houghton BF, Polacci M, Ripepe M (2008) Textural and geophysical characterization of explosive basaltic activity at Villarrica volcano. *Journal of Geophysical Research: Solid Earth* 113(8):1–16. <https://doi.org/10.1029/2007JB005328>

Harris FJ (1978) On the use of windows for harmonic analysis with the discrete Fourier transform. *Proc IEEE* 66(1):51–83. <https://doi.org/10.1109/PROC.1978.10837>

Harris AJL, Carniel R, Jones J (2005) Identification of variable convective regimes at Erta Ale lava lake. *J Volcanol Geoth Res* 142(3–4):207–223. <https://doi.org/10.1016/j.jvolgeores.2004.11.011>

Iezzi AM, Fee D, Kim K, Jolly AD, Mattoza RS (2019) Three-dimensional acoustic multipole waveform inversion at Yasur Volcano, Vanuatu. *Journal of Geophysical Research: Solid Earth* 124(8):8679–8703. <https://doi.org/10.1029/2018JB017073>

Johnson JB, Palma JL (2015) Lahar infrasound associated with Volcán Villarrica's 3 March 2015 eruption. *Geophys Res Lett* 42(15):6324–6331. <https://doi.org/10.1002/2015GL065024>

Johnson JB, Ripepe M (2011) Volcano infrasound: a review. *J Volcanol Geoth Res* 206(3–4):61–69. <https://doi.org/10.1016/j.jvolgeores.2011.06.006>

Johnson J, Aster R, Jones KR, Kyle P, McIntosh B (2008) Acoustic source characterization of impulsive Strombolian eruptions from the Mount Erebus lava lake. *J Volcanol Geoth Res* 177(3):673–686. <https://doi.org/10.1016/j.jvolgeores.2008.06.028>

Johnson JB, Lees J, Varley N (2011) Characterizing complex eruptive activity at Santiaguito, Guatemala using infrasound semblance in networked arrays. *J Volcanol Geotherm Res* 199:1–14. <https://doi.org/10.1016/j.jvolgeores.2010.08.005>

Johnson JB, Ruiz MC, Ortiz HD, Watson LM, Viracocha G, Ramon P, Almeida M (2018a) Infrasound Tornillos produced by Volcán Cotopaxi's Deep Crater. *Geophys Res Lett* 45(11):5436–5444. <https://doi.org/10.1029/2018GL077766>

Johnson JB, Watson LM, Palma JL, Dunham EM, Anderson JF (2018b) Forecasting the eruption of an open-vent volcano using resonant infrasound tones. *Geophys Res Lett* 45(5):2213–2220. <https://doi.org/10.1029/2017GL076506>

Johnson J, Watson L (2019) Monitoring volcanic craters with infrasound “music.” *Eos*, 100 (March). <https://doi.org/10.1029/2019eo123979>

Kim K, Lees JM (2011) Finite-difference time-domain modeling of transient infrasonic wavefields excited by volcanic explosions. *Geophys Res Lett* 38(6):2–6. <https://doi.org/10.1029/2010GL046615>

Kim K, Lees JM (2014) Local volcano infrasound and source localization investigated by 3D simulation. *Seismol Res Lett* 85(6):1177–1186. <https://doi.org/10.1785/0220140029>

Kim K, Lees JM, Ruiz M (2012) Acoustic multipole source model for volcanic explosions and inversion for source parameters. *Geophys J Int* 191(3):1192–1204. <https://doi.org/10.1111/j.1365-246X.2012.05696.x>

Lacanna G, Ripepe M (2013) Influence of near-source volcano topography on the acoustic wavefield and implication for source modeling. *J Volcanol Geoth Res* 250:9–18. <https://doi.org/10.1016/j.jvolgeores.2012.10.005>

Lev E, Ruprecht P, Oppenheimer C, Peters N, Patrick M, Hernández PA, Spampinato L, Marlow J (2019) A global synthesis of lava lake dynamics. *J Volcanol Geoth Res* 381:16–31. <https://doi.org/10.1016/j.jvolgeores.2019.04.010>

Maher S P, Mattoza R S, De Groot-Hedlin C, Kim K, Gee K L (2021) Evaluating the applicability of a screen diffraction approximation to local volcano infrasound. *Volcanica* 4(1). <https://doi.org/10.30909/vol.04.01.6785>

Marchetti E, Ripepe M, Harris AJL, Delle Donne D (2009) Tracing the differences between Vulcanian and Strombolian explosions using infrasonic and thermal radiation energy. *Earth Planet Sci Lett* 279(3–4):273–281. <https://doi.org/10.1016/j.epsl.2009.01.004>

McKee K, Fee D, Yokoo A, Mattoza RS, Kim K (2017) Analysis of gas jetting and fumarole acoustics at Aso Volcano, Japan. *J Volcanol Geoth Res* 340:16–29. <https://doi.org/10.1016/j.jvolgeores.2017.03.029>

Mora-Stock C, Thorwart M, Wunderlich T, Bredemeyer S, Hansteen TH, Rabbel W (2014) Comparison of seismic activity for Llaima and Villarrica volcanoes prior to and after the Maule 2010 earthquake. *Int J Earth Sci* 103(7):2015–2028. <https://doi.org/10.1007/s00531-012-0840-x>

Moussallam Y, Bani P, Curtis A, Barnie T, Moussallam M, Peters N, Schipper CI, Aiuppa A, Giudice G, Amigo A, Velasquez G, Cardona C (2016) Sustaining persistent lava lakes: observations from high-resolution gas measurements at Villarrica volcano, Chile. *Earth Planet Sci Lett* 454:237–247. <https://doi.org/10.1016/j.epsl.2016.09.012>

Naranjo J A, Moreno H (2016) Laharic debris-flows from Villarrica Volcano. Villarrica Volcano (39.5° S), Southern Andes, Chile. Santiago, Servicio Nacional de Geología y Minería 28–45.

Palma JL, Calder ES, Basualto D, Blake S, Rothery DA (2008) Correlations between SO_2 flux, seismicity, and outgassing activity at the open vent of Villarrica volcano, Chile. *Journal of Geophysical Research: Solid Earth* 113(10):1–23. <https://doi.org/10.1029/2008JB005577>

Patrick MR, Anderson KR, Poland MP, Orr TR, Swanson DA (2015) Lava lake level as a gauge of magma reservoir pressure and eruptive hazard. *Geology* 43(9):831–834. <https://doi.org/10.1130/G36896.1>

Pouplet A, Bram K (2021) Nyiragongo and Nyamuragira: a review of volcanic activity in the Kivu rift, western branch of the East African Rift System. *Bulletin of Volcanology* 83(2). <https://doi.org/10.1007/s00445-021-01435-6>

Riad SM (1986) The deconvolution problem: an overview. *Proc IEEE* 74(1):82–85. <https://doi.org/10.1109/PROC.1986.13407>

Richardson JP, Waite GP (2013) Waveform inversion of shallow repetitive long period events at Villarrica Volcano, Chile. *Journal of Geophysical Research: Solid Earth* 118(9):4922–4936. <https://doi.org/10.1002/jgrb.50354>

Richardson JP, Waite GP, Palma JL (2014) Varying seismic-acoustic properties of the fluctuating lava lake at Villarrica volcano, Chile. *AGU: Journal of Geophysical Research. Solid Earth* 119:3678–3699. <https://doi.org/10.1002/2014JB011002>

Ripepe M, Marchetti E, Bonadonna C, Harris AJL, Pioli L, Ulivieri G (2010) Monochromatic infrasonic tremor driven by persistent degassing and convection at Villarrica Volcano. *Chile Geophysical Research Letters* 37(15):2–7. <https://doi.org/10.1029/2010GL043516>

Romero JE, Vera F, Polacci M, Morgavi D, Arzilli F, Alam MA, Bustillos JE, Guevara A, Johnson JB, Palma JL, Burton M, Cuenca E, Keller W (2018) Tephra from the 3 March 2015 sustained column related to explosive lava fountain activity at Volcán Villarrica (Chile). *Front Earth Sci* 6(July):1–14. <https://doi.org/10.3389/feart.2018.00098>

Sawyer GM, Carn SA, Tsanev VI, Oppenheimer C, Burton M (2008) Investigation into magma degassing at Nyiragongo volcano, Democratic Republic of the Congo. *Geochem Geophys Geosyst* 9(2):1–17. <https://doi.org/10.1029/2007GC001829>

Shinohara H, Witter JB (2005) Volcanic gases emitted during mild Strombolian activity of Villarrica volcano. *Chile Geophysical Research Letters* 32(20):1–5. <https://doi.org/10.1029/2005GL024131>

Spina L, Cannata A, Privitera E, Vergniolle S, Ferlito C, Gresta S, Montalto P, Sciutto M (2014) Insights into Mt Etna's shallow plumbing system from the analysis of infrasound signals August 2007–December 2009. *Pure and Applied Geophysics* 172(2):473–490. <https://doi.org/10.1007/s00024-014-0884-x>

Taddeucci J, Alatorre-Ibargüengoitia MA, Moroni M, Tornetta L, Capponi A, Scarlato P, Dingwell DB, De Rita D (2012) Physical parameterization of Strombolian eruptions via experimentally-validated modeling of high-speed observations. *Geophys Res Lett* 39(16):2–7. <https://doi.org/10.1029/2012GL052772>

Van Daele M, Moernaut J, Silversmit G, Schmidt S, Fontijn K, Heirman K, Vandoorne W, De Clercq M, Van Acker J, Wolff C, Pino M, Urrutia R, Roberts SJ, Vincze L, De Batist M (2014) The 600 yr eruptive history of Villarrica Volcano (Chile) revealed by annually laminated lake sediments. *Bulletin of the Geological Society of America* 126(3–4):481–498. <https://doi.org/10.1130/B30798.1>

Vergniolle S, Bouche E (2016) Gas-driven lava lake fluctuations at Erta 'Ale volcano (Ethiopia) revealed by MODIS measurements. *Bulletin of Volcanology* 78(9). <https://doi.org/10.1007/s00445-016-1047-y>

Vergniolle S, Caplan-Auerbach J (2004) Acoustic measurements of the 1999 basaltic eruption of Shishaldin volcano, Alaska 2. Precursor to the Subplinian phase. *Journal of Volcanology and Geothermal Research*, 137(1–3 SPEC. ISS.):135–151. <https://doi.org/10.1016/j.jvolgeores.2004.05.004>

Vergniolle S, Caplan-Auerbach J (2006) Basaltic thermals and Subplinian plumes: constraints from acoustic measurements at Shishaldin volcano. *Alaska Bull Volcanol* 68(7–8):611–630. <https://doi.org/10.1007/s00445-005-0035-4>

Vergniolle S, Métrich N (2022) An interpretative view of open-vent volcanoes. Volc., in press, Bull. <https://doi.org/10.1007/s00445-022-01581-5>

Vergniolle S, Brandeis G, (1994) Origin of the sound generated by Strombolian explosions. *Geophys Res Lett* 21(18):1959–1962. <https://doi.org/10.1029/94GL01286>

Wang S (1996) Finite-difference time-domain approach to underwater acoustic scattering problems. *The Journal of the Acoustical Society of America* 99(4):1924–1931. <https://doi.org/10.1121/1.415375>

Watson LM, Dunham EM, Johnson JB (2019) Simulation and inversion of harmonic infrasound from open-vent volcanoes using an efficient quasi-1D crater model. *J Volcanol Geoth Res* 380:64–79. <https://doi.org/10.1016/j.jvolgeores.2019.05.007>

Watson LM, Johnson JB, Sciutto M, Cannata A (2020) Changes in crater geometry revealed by inversion of harmonic infrasound observations: 24 December 2018 eruption of Mount Etna, Italy. *Geophysical Research Letters* 47(19):1–12. <https://doi.org/10.1029/2020GL088077>

Witsil AJC, Johnson JB (2018) Infrasound explosion and coda signal investigated with joint analysis of video at Mount Erebus, Antarctica. *J Volcanol Geoth Res* 357:306–320. <https://doi.org/10.1016/j.jvolgeores.2018.05.002>

Witter JB, Kress VC, Delmelle P, Stix J (2004) Volatile degassing, petrology, and magma dynamics of the Villarrica Lava Lake, Southern Chile. *J Volcanol Geoth Res* 134(4):303–337. <https://doi.org/10.1016/j.jvolgeores.2004.03.002>

Yokoo A, Ishii K, Ohkura T, Kim K (2019) Monochromatic infrasound waves observed during the 2014–2015 eruption of Aso volcano, Japan. *Earth, Planets and Space* 71(1). <https://doi.org/10.1186/s40623-019-0993-y>

Springer Nature or its licensor (e.g. a society or other partner) holds exclusive rights to this article under a publishing agreement with the author(s) or other rightsholder(s); author self-archiving of the accepted manuscript version of this article is solely governed by the terms of such publishing agreement and applicable law.